Article

Solution-Based Growth and Structural Characterization of Homo- and Heterobranched Semiconductor Nanowires

Angang Dong, Rui Tang, and William E. Buhro

J. Am. Chem. Soc., **2007**, 129 (40), 12254-12262• DOI: 10.1021/ja0737772 • Publication Date (Web): 19 September 2007

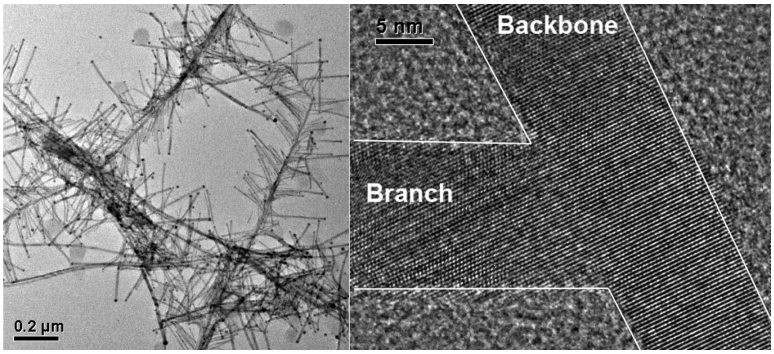

More About This Article

Additional resources and features associated with this article are available within the HTML version:

- Supporting Information
- Links to the 9 articles that cite this article, as of the time of this article download
- Access to high resolution figures
- Links to articles and content related to this article
- Copyright permission to reproduce figures and/or text from this article

View the Full Text HTML

J|A|C|S
ARTICLES
Published on Web 09/19/2007

Solution-Based Growth and Structural Characterization of Homo- and Heterobranched Semiconductor Nanowires

Angang Dong, Rui Tang, and William E. Buhro*

Contribution from the Department of Chemistry and Center for Materials Innovation, Washington University, St. Louis, Missouri 63130-4899

Received May 25, 2007; E-mail: buhro@wustl.edu

Abstract: Colloidal homobranched ZnSe nanowires (NWs) and heterobranched CdSe−ZnSe NWs are successfully synthesized by combining a sequential seeding strategy with the solution−liquid−solid (SLS) growth process. We have developed an efficient approach to deposit secondary bismuth nanoparticles onto the NW backbone to induce the subsequent SLS branch growth. The density, length, and diameter of branches are rationally controlled by varying reaction conditions. Structural characterization reveals that crystalline branches grow epitaxially from the backbone in both homo- and heterobranched NWs. Two different branching structures are observed in the CdSe−ZnSe heterobranched NWs, owing to the phase admixture, i.e., cubic and hexagonal crystal structures, coexisting in the CdSe NW backbones. These branched NWs with well-designed architectures are expected to have potential as three-dimensional building blocks in the fabrication of nanoscale electronics and photonics.

Introduction

We report formation of colloidal homo- and heterobranched semiconductor nanowires by applying a stepwise seeding strategy in the solution−liquid−solid process. ZnSe was chosen to demonstrate the growth of homobranched nanowires, whereas CdSe and ZnSe served as the backbone and branch materials, respectively, in the synthesis of CdSe−ZnSe heterobranched nanowires. In both cases, rational control over the branching morphology, including the branch density, length, and diameter, was readily achieved by optimizing reaction conditions. High-resolution transmission electron microscopy (HRTEM) images and fast Fourier transforms (FFTs) confirmed that crystalline branches grew epitaxially from the backbone, with branching angles having crystallographically determined values.

Semiconductor nanowires (NWs) represent an important class of low-dimensional nanomaterials that have significant promise as building blocks in the bottom-up construction of nanoscale electronic and photonic devices.[1] The realization of these devices ultimately relies on the ability to control the composition, morphology, interconnection, and integration of the NW building blocks.[2−4] To this end, a number of synthetic strategies[4−6] have been developed in the past few years to make high-quality semiconductor NWs with various compositions, the availability of which opens up many new opportunities for both fundamental research[7,8] and technological applications.[9−11]

Recently, semiconductor NWs with greater complexity have become increasingly important to the development of nanoscale devices, as these complex nanostructures introduce further opportunities for enhancing device functionality.[12−17] For example, semiconductor NWs with either radial[12,13] (core−shell heterostructures) or axial[14−17] (longitudinal) heterojunctions have been synthesized by the vapor−liquid−solid (VLS)[12−15] and solution−liquid−solid (SLS)[16,17] growth processes and have already been utilized to fabricate nanoscale devices such as single-NW light-emitting diodes (LEDs) and high-performance field effect transistors (FETs), etc.[15] Yet these heterostructured NW building blocks are still simple in terms of dimensionality and morphology despite the compositional complexity, which will inevitably limit their applications, especially in devices requiring three-dimensional (3D) NW interconnections or networks as building blocks.[3]

(1) Law, M.; Goldberger, J.; Yang, P. *Annu. Rev. Mater. Res.* **2004**, *34*, 83.
(2) Javey, A.; Nam, S. W.; Friedman, R. S.; Yan, H.; Lieber, C. M. *Nano Lett.* **2007**, *7*, 773.
(3) Wang, D.; Lieber, C. M. *Nature Mater.* **2003**, *2*, 355.
(4) Duan, X.; Lieber, C. M. *Adv. Mater.* **2000**, *12*, 298.
(5) Holmes, J. D.; Johnston, K. P.; Doty, R. C.; Korgel, B. A. *Science* **2000**, *287*, 1471.
(6) Wang, F.; Dong, A.; Sun, J.; Tang, R.; Yu, H.; Buhro, W. E. *Inorg. Chem.* **2006**, *45*, 7511.
(7) Yu, H.; Li, J.; Loomis, R. A.; Wang, L.; Buhro, W. E. *Nature Mater.* **2003**, *2*, 517.
(8) Yu, H.; Li, J.; Loomis, R. A.; Gibbons, P. C.; Wang, L.; Buhro, W. E. *J. Am. Chem. Soc.* **2003**, *125*, 16168.
(9) (a) Huang, M. H.; Mao, S.; Feick, H.; Yan, H.; Wu, Y.; Kind, H.; Weber, E.; Russo, R.; Yang, P. *Science* **2001**, *292*, 1897. (b) Law, M.; Sirbuly, D. J.; Johnson, J. C.; Goldberger, J.; Saykally, R. J.; Yang, P. *Science* **2004**, *305*, 1269.
(10) (a) Yang, R.; Chueh, Y.; Morber, J. R.; Snyder, R.; Chou, L.; Wang, Z. L. *Nano Lett.* **2007**, *7*, 269. (b) Wang, Z. L.; Song, J. *Science* **2006**, *312*, 242. (c) Wang, X.; Song, J.; Liu, J.; Wang, Z. L. *Science* **2007**, *316*, 102.
(11) Li, Y.; Qian, F.; Xiang, J.; Lieber, C. M. *Mater. Today* **2006**, *9*, 18.
(12) Lauhon, L. J.; Gudiksen, M. S.; Wang, D.; Lieber, C. M. *Nature* **2002**, *420*, 57.
(13) Yin, L.; Li, M.; Bando, Y.; Golberg, D.; Yuan, X.; Sekiguchi, T. *Adv. Funct. Mater.* **2007**, *17*, 270.
(14) Björk, M. T.; Ohlsson, B. J.; Sass, T.; Persson, A. I.; Thelander, C.; Magnusson, M. H.; Deppert, K.; Wallenberg, L. R.; Samuelson, L. *Nano Lett.* **2002**, *2*, 87.
(15) Gudiksen, M. S.; Lauhon, L. J.; Wang, J.; Smith, D. C.; Lieber, C. M. *Nature* **2002**, *415*, 617.
(16) Ouyang, L.; Maher, K. N.; Yu, C. L.; McCarty, J.; Park, H. *J. Am. Chem. Soc.* **2007**, *129*, 133.
(17) Dong, A.; Wang, F.; Daulton, T. L.; Buhro, W. E. *Nano Lett.* **2007**, *5*, 1308.

10.1021/ja0737772 CCC: $37.00

Very recently, branched and hyperbranched semiconductor nanocrystals or NWs have been emerging as a unique and important class of 3D interconnecting building blocks to enable much greater functionality.[18−27] Several groups have reported the synthesis of branched semiconductor NWs with various compositions, the growth of which generally relies on a multistep metal-nanoparticle-seeded VLS process.[18−21] In addition to the vapor-phase approaches, some groups have developed *solution-based* synthetic strategies to produce branched nanocrystals or NWs.[23−27] For example, Alivisatos and co-workers have synthesized hyperbranched CdTe and CdSe nanocrystals with independently controlled branching density and branch length by varying the amount and kind of surface-capping agents.[23,24] In the case of NWs, Kuno and co-workers have reported the solution-phase synthesis of branched CdSe,[25] PbSe,[26] and CdTe[27] NWs through variations of the precursor ratios and/or surface-capping ligands. However, the latter study has a limited control over the branching density, branching angle, and branch length and diameter,[25−27] which may be crucial to the rational design of NW building blocks.[18]

In this work, we report the rational synthesis of homo- and heterobranched semiconductor NWs by applying a sequential seeding strategy in the SLS growth process. ZnSe homobranched NWs and CdSe−ZnSe heterobranched NWs were grown to demonstrate the method. Rational control over the branching morphology, i.e., the density, length, and diameter of branches, can be readily achieved by optimizing reaction conditions. To obtain a high branching yield, we have developed an efficient approach to deposit secondary bismuth (Bi) nanoparticles onto the preformed NW backbones to induce the subsequent branch growth. HRTEM studies and the corresponding 2D FFTs revealed that single-crystalline branches grew from the backbone via an epitaxial process in both homobranched and heterobranched NWs. To our knowledge, this is the first report of the rational growth of branched semiconductor NWs through a solution-based approach. Compared to the conventional VLS method, the SLS process generally offers backbone and branch NWs with much smaller diameters within the quantum-confinement regime,[25−27] which should open up avenues for investigating the size- and shape-dependent optical and electrical properties of these novel complex NW architectures.

Experimental Section

Chemicals. The following chemicals were purchased and used as received unless otherwise noted. Zinc stearate ($Zn(SA)_2$, 99%) was obtained from Alfa Aesar. Cadmium oxide (CdO, 99.99%), tri-*n*-octylphosphine (TOP, 90%), tri-*n*-octylphosphine oxide (TOPO, 99%), tri-*n*-butylphosphine (TBP, 97%), 1-hexadecylamine (HDA, 98%), 1-octadecene (ODE, 90%), elemental Se powder, oleic acid (OA, 90%), polyethylenimine (PEI, M_n = 600 by GPC), poly(1-hexadecene)$_{0.67}$-*co*-(1-vinylpyrrolidinone)$_{0.33}$, and $Na[N(SiMe_3)_2]$ (1.0 M solution in THF) were purchased from Aldrich. 1,3-Diisopropylbenzene (DIPB, from Aldrich) was shaken with concentrated sulfuric acid to remove thiophene, washed with water, and distilled over Na.

All preparative procedures were conducted using standard Schlenk-line techniques in dry glassware under a dry N_2(g) atmosphere.

Preparation of the Bi Nanoparticle Stock Solutions. Monodispersed Bi nanoparticles were grown in DIPB solutions of poly(1-hexadecene)$_{0.67}$-*co*-(1-vinylpyrrolidinone)$_{0.33}$ and $Na[N(SiMe_3)_2]$ at elevated temperatures (170−210 °C), as previously reported.[8,17] The diameter of the Bi nanoparticles was tuned from 4 to 22 nm (standard deviation = 5−10% in mean diameter) by varying reaction conditions, and the effective concentration of the dispersions was 0.04 mmol of Bi/g of DIPB.

Preparation of ZnSe and CdSe NW Backbones. Both ZnSe[17] and CdSe[8] NWs were synthesized by the Bi-seeded SLS growth process, following the respective procedures we previously reported. After synthesis, the NW product was purified and redispersed in toluene or chloroform for future use. ZnSe NWs (mean diameter = 10−14 nm) obtained by this method mainly possess a cubic crystal structure with a growth axis along the [111] lattice direction, whereas cubic and hexagonal crystal phases coexist in CdSe NWs (mean diameter = 6−12 nm), and the wire growth axis is along the [111] (for cubic) or [002] (for hexagonal) lattice direction.[25]

Synthesis of Homobranched ZnSe NWs. To synthesize branched ZnSe NWs, the surface of the original ZnSe NW backbones was first coated by PEI to form PEI-coated NWs. In a typical procedure, PEI (∼0.1 mL, 0.00018 mmol) was added to the chloroform solution (∼2 mL) of the purified ZnSe NWs (0.1 mmol based on the assumption of a complete reaction between $Zn(SA)_2$ and TOPSe),[17] following the literature procedure[28] with a little modification. The resulting solution mixture was sonicated in a cleaning bath at room temperature for 30 min to ensure completeness of PEI coating. (TEM images taken before and after the sonication step revealed no evidence of NW breakage or shortening under the conditions employed.) Toluene (∼3 mL) was then added to precipitate ZnSe NWs, and the precipitated NWs, collected by centrifugation, were redissolved in methanol (∼3 mL), indicating the attachment of PEI to the NW surface. To the methanol solution of the PEI-coated ZnSe NWs was added a certain amount of Bi-seed stock solution (10−40 mg, 0.0004−0.0016 mmol, mean diameter = 5−20 nm), leading to the coprecipitation of both NWs and Bi seeds. The ZnSe NW−Bi precipitate collected by centrifugation was dispersed in ODE (∼2 mL) in a Schlenk reaction tube, and the resultant dispersion was then annealed at 300 °C for 2 min under N_2(g). Afterward, $Zn(SA)_2$ (0.025−0.1 mmol), TOPSe (0.15−0.6 mmol, freshly prepared by dissolving Se powder in TOP at room temperature), and surface-capping ligands TOPO (0.13−0.52 mmol) and HDA (0.04−0.16 mmol) were introduced to induce the growth of ZnSe branches, following the previously reported procedure for ZnSe NW growth.[17] After 5 min of growth, the reaction tube was withdrawn and allowed to cool to room temperature. The branched NW product was purified by addition of a mixture of toluene (∼1 mL) and methanol (∼2 mL), and the precipitated product, collected by centrifugation, was dissolved in chloroform (∼2 mL).

Synthesis of Heterobranched CdSe−ZnSe NWs. As for the growth of homobranched ZnSe NWs, a PEI-coating step was conducted on the initial CdSe NWs, followed by annealing the CdSe NW−Bi composite in ODE at 300 °C for 2 min. The subsequent ZnSe branch growth and purification procedures were performed in the same way as described above for homobranched ZnSe NWs.

(18) Wang, D.; Qian, F.; Yang, C.; Zhong, Z.; Lieber, C. M. *Nano Lett.* **2004**, *4*, 871.
(19) (a) Dick, K. A.; Deppert, K.; Larsson, M. W.; Martensson, T.; Seifert, W.; Wallenberg, L. R.; Samuelson, L. *Nature Mater.* **2004**, *3*, 380. (b) Dick, K. A.; Deppert, K.; Karlsson, L. S.; Seifert, W.; Wallenberg, L. R.; Samuelson, L. *Nano Lett.* **2006**, *6*, 2842.
(20) Zhu, J.; Peng, H.; Chan, C. K.; Jarausch, K.; Zhang, X. F.; Cui, Y. *Nano Lett.* **2007**, *7*, 1095.
(21) Jung, Y.; Ko, D.; Agarwal, R. *Nano Lett.* **2007**, *7*, 264.
(22) May, S. J.; Zheng, J.; Wessels, B. W.; Lauhon, L. J. *Adv. Mater.* **2005**, *17*, 598.
(23) Manna, L.; Milliron, D. J.; Meisel, A.; Scher, E. C.; Alivisatos, A. P. *Nature Mater.* **2003**, *2*, 382.
(24) Kanaras, A. G.; Sonnichsen, C.; Liu, H.; Alivisatos, A. P. *Nano Lett.* **2005**, *5*, 2164.
(25) Grebinski, J. W.; Hull, K. L.; Zhang, J.; Kosel, T. H.; Kuno, M. *Chem. Mater.* **2004**, *16*, 5260.
(26) Hull, K. L.; Grebinski, J. W.; Kosel, T. H.; Kuno, M. *Chem. Mater.* **2005**, *17*, 4416.
(27) Kuno, M.; Ahmad, O.; Protasenko, V.; Bacinello, D.; Kosel, T. H. *Chem. Mater.* **2006**, *18*, 5722.
(28) Nann, T. *Chem. Commun.* **2005**, 1735.

Characterization. Low-resolution TEM images and energy-dispersive X-ray spectroscopy (EDS) were recorded using a JEOL 2000 FX microscope operating at 200 kV. HRTEM images were conducted on a JEOL JEM-2100F microscope operating at 200 kV. Samples for TEM and HRTEM were prepared by dropping a dilute chloroform solution of branched NWs on ultrathin carbon film-coated Cu TEM grids. The branch lengths and diameters and branching angles were measured and recorded using Image-Pro Express software (version 4.5). UV−visible absorption spectra were acquired using a Varian Cary 1E spectrophotometer. Photoluminescence (PL) emission spectra were taken at room temperature on a Varian Cary Eclipse fluorescence spectrophotometer.

Results and Discussion

Homobranched ZnSe NWs. To enable branch growth, the first step was to deposit secondary Bi nanoparticles onto the preformed ZnSe NW backbones. In the VLS growth of branched NWs, metal nanoparticles are usually directly deposited from solution[18] or aerosol[19] onto the NW backbones, which are grown on substrate. Once deposited, the attached metal seeds do not detach from the NW surface prior to the branch growth. However, this simple metal-seed-deposition approach was not applicable to the SLS growth process, as the Bi nanoparticles are solvent dispersible and easily detached from the NW surface prior to the branch growth, diffusing into the reaction solution. As a result, a high branching yield was not obtained.

In our initial attempts to attach Bi seeds to the ZnSe NW backbones, the Bi-nanoparticle stock solution was mixed directly with the purified ZnSe NWs dissolved in toluene, and the subsequent addition of methanol led to the coprecipitation of both Bi nanoparticles and ZnSe NWs. To ensure a firmer attachment of Bi seeds, the ZnSe NW−Bi composite was further annealed in ODE at 300 °C. However, most of the Bi seeds remained unattached to the NW surface even after annealing (Figure S1, Supporting Information), indicating a poor seed-deposition efficiency. We attributed this to the weak interaction between the NW surface and Bi nanoparticles. Because the original NWs were capped by TOPO, TOP, and HDA molecules, all of which have long hydrocarbon tails extending outward, we surmised that the NW backbone exhibited a weak affinity toward the Bi nanoparticles, leading to a low attachment yield of the Bi seeds. Therefore, an efficient way to increase the attachment yield of the Bi seeds was prerequisite to achieving a high branching yield.

One advantage of the SLS growth process over the conventional VLS process is that the NW surface properties can be easily modified by changing the surface-capping ligands. We found that PEI-coated NWs showed a high affinity toward Bi nanoparticles, and a firmer attachment of Bi seeds was achieved by the subsequent annealing step in ODE. PEI is a hyperbranched polymer, soluble in chloroform, methanol, and water, but insoluble in toluene, and has been used in the preparation of water-soluble quantum dots by phase-transfer reactions.[28] We attributed the efficient attachment of Bi seeds to the PEI-coated NWs to the following reasons. First, Bi nanoparticles can become entangled with the long and flexible polymer chains attached to the NW surface, thus decreasing the possibility of detachment of Bi seeds during the subsequent annealing process. Second, the abundant primary, secondary, and tertiary amine groups on the PEI chains should coordinate with Bi, further enhancing the interaction between the NW surface and the Bi seeds.

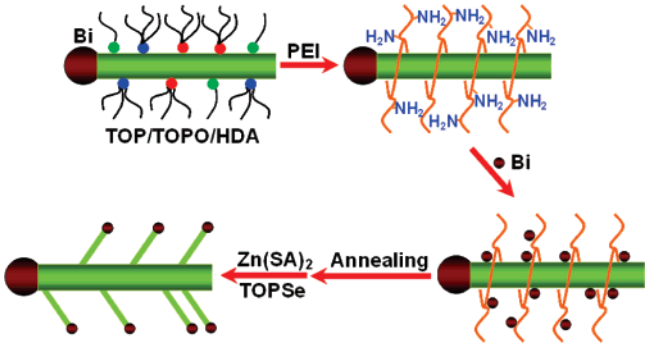

Figure 1. Schematic illustration of the synthesis of homobranched ZnSe NWs by applying a stepwise seeding strategy in the SLS growth process.

Figure 1 schematically illustrates our approach for the synthesis of homobranched ZnSe NWs. The NWs were coated by PEI, upon which the NWs became methanol soluble and toluene insoluble, establishing the success of the coating process. Bi seeds were subsequently deposited, affording NWs with loosely associated Bi seeds (images not shown), suggesting that the seeds were entangled in the PEI coatings. The ZnSe NW−Bi composite was then annealed in ODE to firmly attach the Bi seeds to the NW surface. Finally, branches were grown by the SLS process to obtain the branched NW structures. The branched NWs regained toluene solubility, indicating that the PEI coatings were partially or fully dissociated during the annealing or subsequent branch-growth steps.

A typical TEM image (Figure 2a) of the annealed ZnSe NW−Bi composite demonstrates that most secondary Bi seeds (∼7 nm in diameter) were successfully deposited onto the NW surface, although their original spherical shape was somewhat changed in the high-temperature annealing process, indicating a high yield of Bi-seed attachment. HRTEM studies demonstrated that part of the Bi nanoparticle appeared to penetrate into the ZnSe NW lattice after annealing (Figure 2b), confirming a firm attachment of Bi seeds to the NW backbone.

The branched ZnSe NWs were first investigated by TEM. Figure 3a is a representative low-magnification TEM image of an ensemble of branched NWs, showing a high branching yield and therefore a good efficiency of the seed-deposition approach. The branch lengths ranged from 200 to 300 nm, with a mean branch diameter of 7.2 ± 1.4 nm (Figure S2, Supporting Information). Bi nanoparticles were easily observed at the branch tips, confirming that the branch growth was initiated by the secondary Bi seeds through the SLS process. The optical properties of the branched ZnSe NWs were examined by UV−visible absorption and PL emission spectroscopies. The absorption spectrum (Figure 3b, blue curve) measured from the same sample exhibited a first excitonic feature around 450 nm, which is slightly blue-shifted with respect to the bulk band gap of ZnSe (∼460 nm),[29] due to a weak quantum-confinement effect.[17] The PL spectrum (Figure 3b, red curve) of the branched NWs showed a peak at ∼460 nm, attributed to the band-edge emission of the ZnSe NWs.

Although precise control over the position of Bi seeds on the NW backbone cannot be achieved at present, the branching density was easily modulated by varying the number of Bi seeds deposited onto the NW backbone (i.e., the amount of the Bi seeds employed during the seed-deposition step). Figure 4 shows

(29) Yoffe, A. D. *Adv. Phys.* **2002**, *51*, 799.

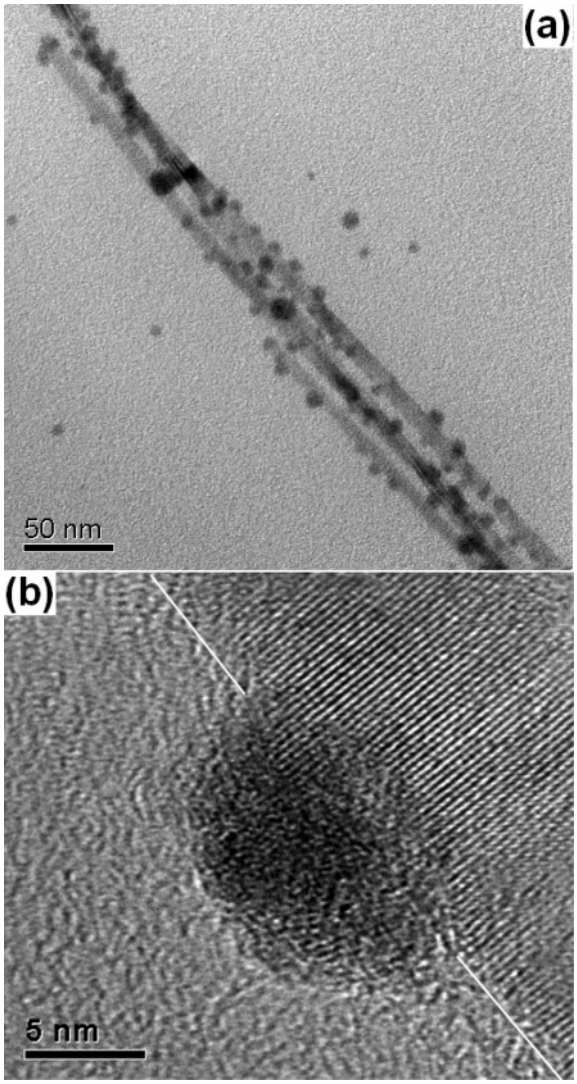

Figure 2. (a) Typical TEM image of the ZnSe NW−Bi composite obtained by depositing Bi seeds onto the PEI-coated ZnSe NWs followed by annealing, showing that most Bi seeds were attached to the NW surface. (b) Representative HRTEM image of the same sample, showing that part of the Bi nanoparticle appeared to penetrate into the ZnSe lattice.

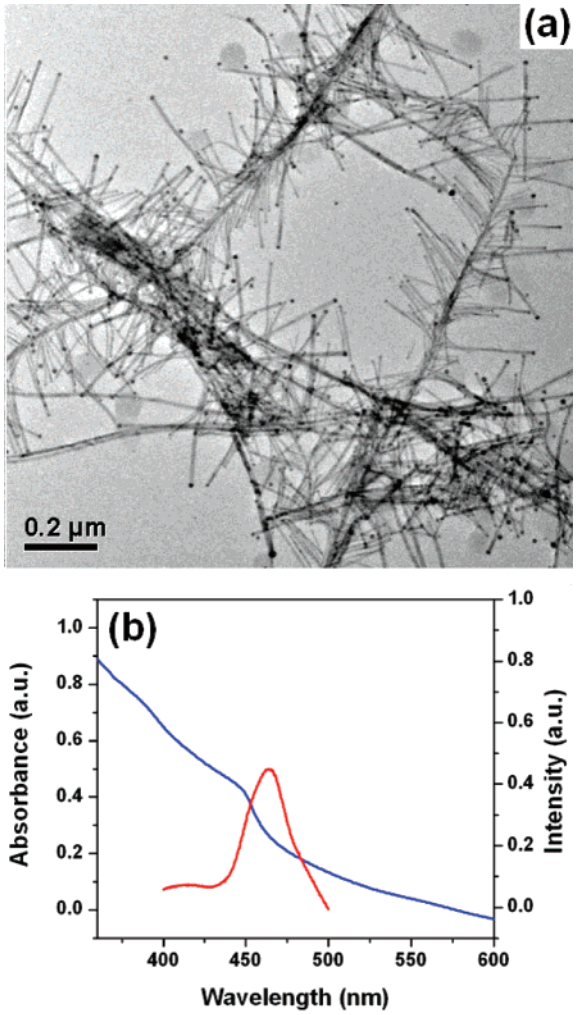

Figure 3. (a) Representative low-magnification TEM image of homo-branched ZnSe NWs. The branch lengths range from 200 to 300 nm, with a mean branch diameter of 7.2 nm. (b) UV−visible absorption spectrum (blue curve) and PL emission spectrum (red curve) of the same sample. The excitation wavelength for PL emission experiments is 340 nm.

two representative TEM images of branched ZnSe NWs having different branching densities, demonstrating a good control of this parameter. The ZnSe branches grew in three planes about the backbone axis, as shown in Figure 4b, in which three sets of branches lying in the different planes are indicated by the red, blue, and green arrows, respectively. This 3D branching behavior is reasonable, considering that a Bi-nanoparticle position on a backbone is initially randomly selected during the seed-deposition process (Figure 2a). Another significant feature observed from Figure 4 is that most branches grew from the backbone with branching angles within a narrow range (i.e., 62−75°). The average branching angle measured from 25 angles was 69.2° ± 4.0°. These observations suggest that the branch growth is through an epitaxial process and there is a certain defined crystallographic relationship between crystalline backbone and branches, which will be discussed in detail below.

The branch diameters were easily tuned by choosing different-sized Bi nanoparticles as the secondary seeds. Figure 5 shows the representative TEM images of branched ZnSe NWs with various mean branch diameters ranging from 5 to 19 nm. These images demonstrate that our approach can produce branched NWs with branch diameters controlled in a similar manner to the previous single-step SLS growth process.[7−8]

In addition to the diameter control, control over the branch lengths was also realized by manipulating the precursor amount. Typical TEM images of branched ZnSe NWs with different mean branch lengths are shown in Figure 6. The branch lengths were varied from 30 to 500 nm. All of the above results demonstrate the capability of our approach to rationally control the morphological features of the branched NWs, which is obviously critical to the design of NW building blocks.

As mentioned above, one significant feature observed in TEM images is that most branches grow with a preferred orientation with respect to the backbone axis, suggesting that the crystalline branch and backbone have a certain defined relationship. To further elucidate this structural relationship, we have used HRTEM to examine the branched NWs. A typical HRTEM image of a single branched ZnSe NW is shown in Figure 7. The clear lattice fringes suggest the high single crystallinity of both backbone and branch, although stacking faults and/or twinnings were frequently observed. The clean backbone−branch junction region indicates the overall structural homo-

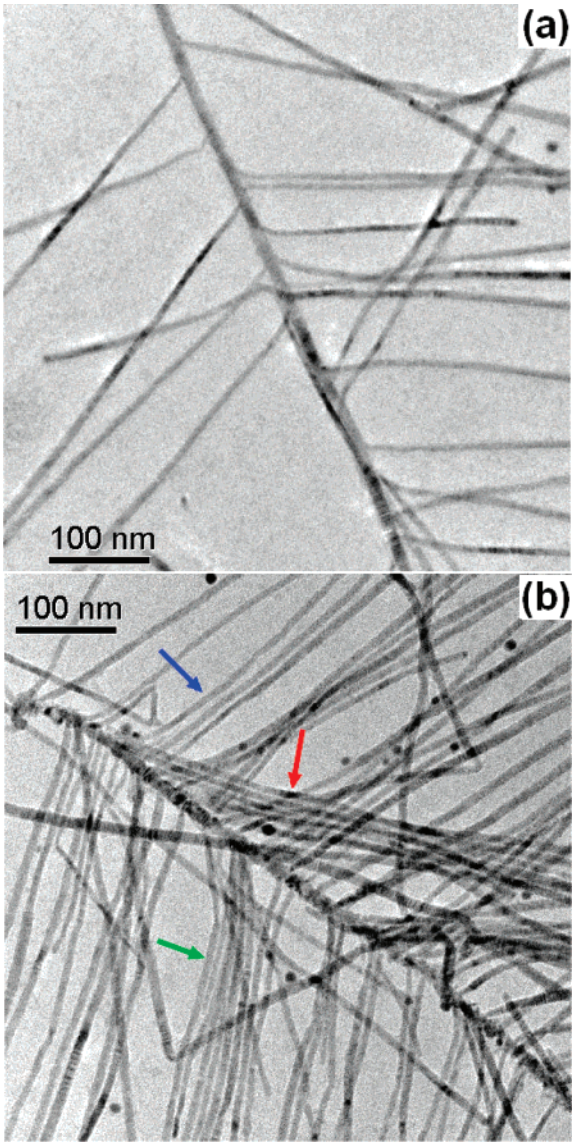

Figure 4. Typical TEM images of homobranched ZnSe NWs with relatively low (a) and high (b) branching densities. The red, blue, and green arrows in (b) indicate three sets of branches lying in three specific planes containing the backbone axis, implying a 3D branching structure.

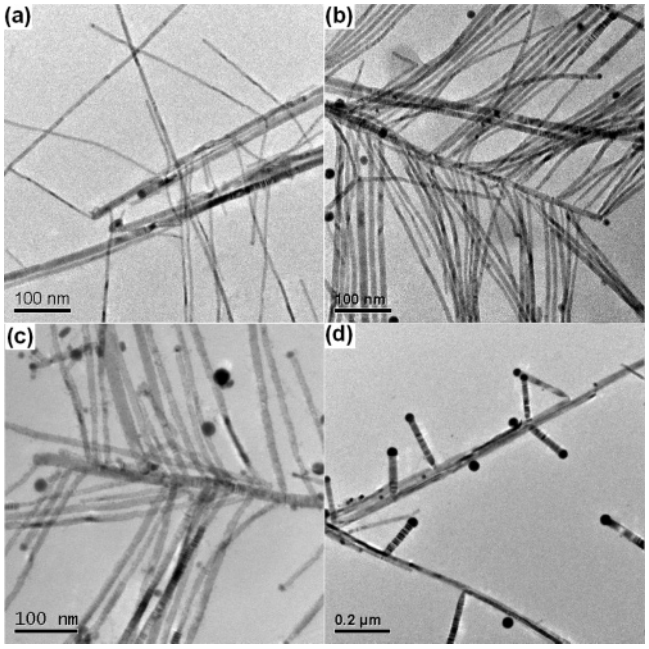

Figure 5. Representative TEM images of homobranched ZnSe NWs with different branch diameters. Mean branch diameters: (a) 4.8 ± 0.7 nm; (b) 7.2 ± 1.4 nm; (c) 11.0 ± 2.2 nm; (d) 18.5 ± 5.0 nm.

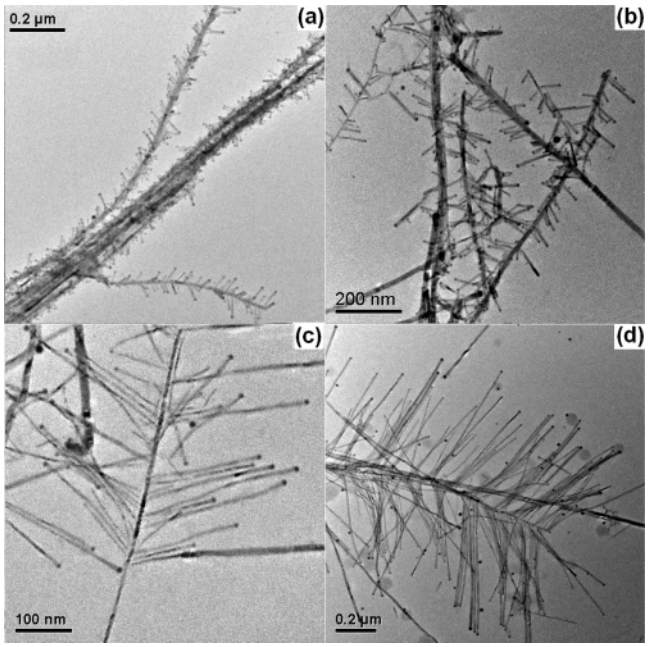

Figure 6. Representative TEM images of homobranched ZnSe NWs with different branch lengths. Mean branch lengths: (a) 29 ± 12 nm; (b) 78 ± 31 nm; (c) 175 ± 56 nm; (d) 437 ± 102 nm.

geneity and the epitaxial branch growth, which was corroborated by the 2D FFTs (Figure 7, insets). The reciprocal lattice peaks in the corresponding FFTs show that both backbone and branch have a cubic crystal structure with growth axes along the $[11\bar{1}]$ and $[\bar{1}1\bar{1}]$ lattice directions, respectively, in the [011] zone axis. The branch-to-backbone angle measured from the lattice peaks is 69.7°, which agrees well with the theoretical value of 70.5° between these two directions. In addition, the FFT (Figure 7, left inset) obtained from the image of the junction region has the same reciprocal lattice peaks as do the FFTs obtained from the images of both backbone (Figure 7, bottom-right inset) and branch regions (Figure 7, upper-right inset), providing further evidence of epitaxial branch growth.

Interestingly, this epitaxial relationship between the cubic-structured backbone and branches suggests that branches can be grown in three possible directions with respect to the backbone axis once the backbone growth direction is defined. These four directions coincide with the growth axes originating from the four identical {111} facets of a tetrahedron in the cubic crystal structure, which is consistent with the observed three branch growth directions shown in Figure 4b. Similar results were also observed by Samuelson and co-workers in the synthesis of branched GaP nanowires by the VLS method.[19a]

Heterobranched CdSe−ZnSe NWs. Conceptually, our approach should be general for the growth of branched NWs with a broad range of compositions, provided that the backbone NWs are stable during the PEI-coating process. To demonstrate its generality, the same methodology was used to grow heterobranched NWs in which the backbone and branches were composed of CdSe and ZnSe, respectively. CdSe NWs have been successfully synthesized by the SLS mechanism, and their

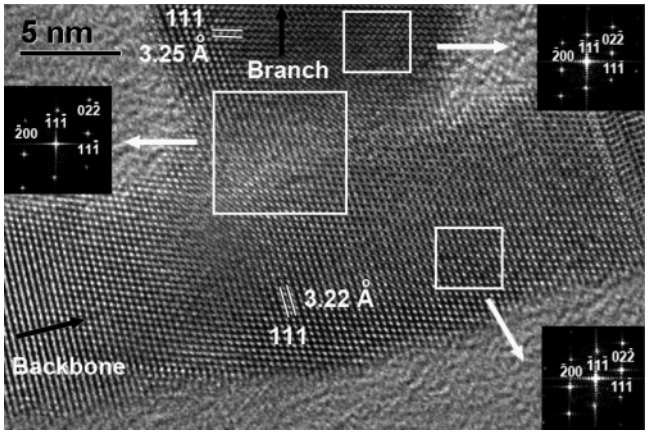

Figure 7. Representative HRTEM image of a single homobranched ZnSe NW. The black arrows display the backbone and branch growth axes. The left, upper-right, and bottom-right insets show the 2D FFTs calculated from the images (indicated by squares) of the junction region, branch region, and backbone region, respectively. Both backbone and branch grow along the ⟨111⟩ lattice direction in the [011] zone axis, determined from the corresponding FFTs. The [111] lattice−fringe spacings (3.25 Å for the branch and 3.22 Å for the backbone) are consistent with the standard value 3.27 Å for cubic-structured ZnSe.

properties have been well studied.[8,25] Similar to the growth of homobranched ZnSe NWs, a PEI-coating step and a subsequent annealing process were performed to ensure a high yield and firm attachment of Bi seeds to the CdSe NW backbones. The following ZnSe-branch growth procedure was carried out in the same way as described above for the homobranched ZnSe NWs.

The strategies used in controlling the branching morphology of the homobranched ZnSe NWs are also applicable to the heterobranched NWs. Figure 8 shows the TEM images of two CdSe−ZnSe branched NW samples having different branching morphologies in terms of branching density, branch length, and branch diameter. Similar to the homobranched ZnSe NWs, the 3D branching morphology was also observed in the CdSe−ZnSe heterobranched NWs, as shown in Figure 8a.

EDS was employed to examine the chemical composition of a single heterobranched NW (Figure 9a), demonstrating that the backbone was composed of CdSe, whereas the branch near the Bi tip was composed of ZnSe, as expected (Figure S3, Supporting Information). An EDS scan analysis (probe size ∼20 nm) revealed that a branch segment near the junction region was composed of alloyed $Zn_{1-x}Cd_xSe$, with x (i.e., the Cd percentage in the branch) gradually decreasing along the branch growth direction and eventually reaching nearly 0 after ∼45 nm, with the disappearance of Cd signal (Figure 9b). This result indicated that Cd ions diffused from the backbone into the branch region in the early branch-growth stage. The formation of such an alloyed segment is believed to relieve the strain caused by lattice mismatch,[21] in this case ∼7% between CdSe and ZnSe.[30] Similar results were also observed by Agarwal and co-workers[21] in the high-temperature (∼740 °C) growth of ZnS−CdS heterobranched NWs by the VLS method.

As for the homobranched ZnSe NWs, ZnSe branches also grew epitaxially from the CdSe backbone, because most branch-to-backbone angles were found to be within a specific range, i.e., 60−70°. Note that, in many cases, a short branch segment (10−30 nm in length) near the junction region was found to

(30) Madelung, O. *Semiconductors−Basic Data*, 2nd revised ed.; Springer: Berlin, 1996.

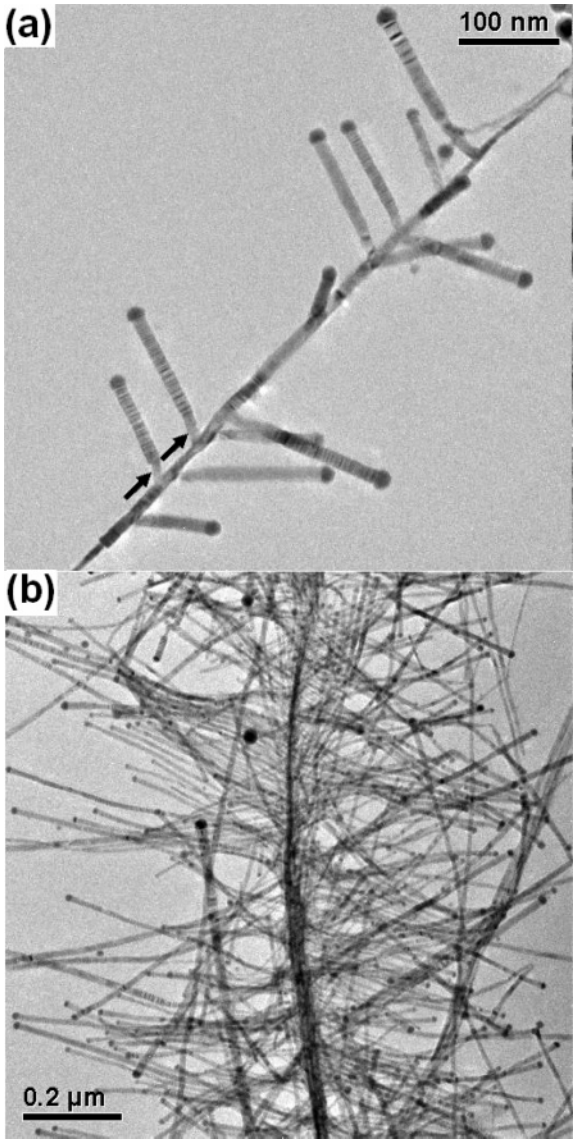

Figure 8. Representative TEM images of heterobranched CdSe−ZnSe NWs with lower branching density and shorter, thicker branches (a), and higher branching density and longer, thinner branches (b). The black arrows in (a) indicate the transitional sections between the backbone and branch.

exhibit a branch-to-backbone angle slightly different from the angle between the remaining branch segment and the backbone (indicated by arrows in Figures 8a and 9a). It seems that this segment is a transitional section from the backbone to branch, and the reason behind this interesting phenomenon will be discussed in detail below. We often observed that the diameter of the transitional segment was smaller than the diameter of the remainder of the branch (see Figures 8a and 9a). The origin of this diameter difference is unknown but may be related to the relative solubilities of ZnSe and CdSe in the (molten) Bi seed.

To gain insightful structural information about heterobranched NWs, HRTEM was performed on the junction region. Interestingly, two different branching structures were normally observed, owing to the admixture of two crystal structures (i.e., cubic and hexagonal) existing in the CdSe NW backbones. This admixture has been commonly found in the SLS-grown CdSe NWs[25] and likely derives from the slight energy difference between cubic and hexagonal crystal phases (2 meV/2 atoms

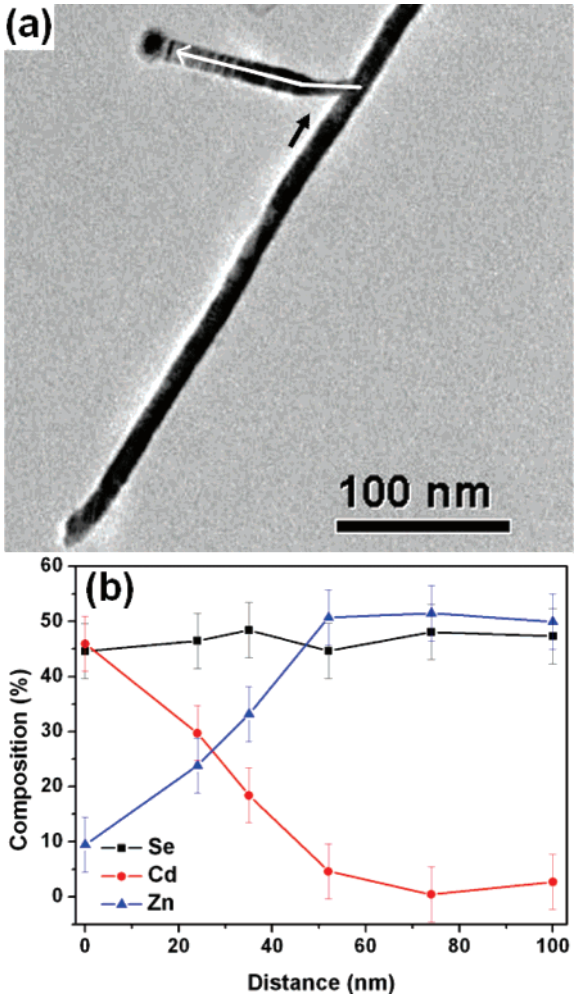

Figure 9. (a) TEM image of a single heterobranched CdSe−ZnSe NW used for the EDS line scan (probe size ∼20 nm) starting from the junction region. The black arrow indicates the transitional branch segment. (b) EDS line profiles of the branched wire in (a), showing the change of composition as function of position and the disappearance of Cd signal in the branch occurring ∼45 nm from the junction region.

for CdSe).[31] Figure 10 shows a typical HRTEM image of a single CdSe−ZnSe branched NW, in which the CdSe backbone (∼9 nm in diameter) has a cubic crystal structure. This image and the corresponding FFTs demonstrate several important points. First, both backbone and branch are single crystalline, having a growth axis along a ⟨111⟩ lattice direction in the [011] zone axis of the cubic crystal structure, despite the stacking faults and/or twinnings, similar to the homobranched ZnSe NWs described above. Second, the clean junction demonstrates the epitaxial branch growth, which was further confirmed by the FFTs obtained from the images of different regions (Figure 10, insets). The branch-to-backbone angle determined from the reciprocal lattice peaks is 73.8°, consistent with the theoretical value of 70.5° between two ⟨111⟩ directions. In some cases, the original stacking faults and/or twinnings existing in the backbone region were entirely inherited in the branch (Figure S4, Supporting Information), also owing to the epitaxial growth process. Third, the [111] lattice−fringe spacings measured from two different regions in the early formed branch segment are 3.40 and 3.33 Å, respectively, consistent with alloyed $Zn_{1-x}Cd_xSe$.

(31) Wei, S-H.; Zhang, S. B. *Phys. Rev. B* **2000**, *62*, 6944.

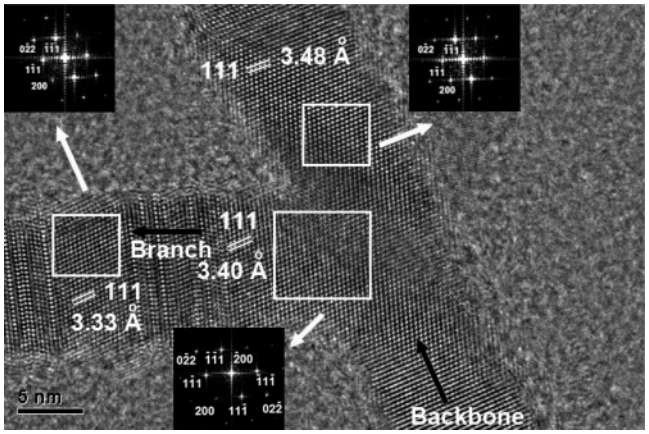

Figure 10. Representative HRTEM image of a single heterobranched CdSe−ZnSe NW in which the CdSe backbone has a cubic crystal structure. The black arrows display the backbone and branch growth axes. The bottom, upper-left, and upper-right insets show the 2D FFTs calculated from the images (indicated by squares) of the junction region, branch region, and backbone region, respectively. Both backbone and branch grow along the ⟨111⟩ lattice direction in the [011] zone axis, determined from the corresponding FFTs. The FFT (bottom inset) obtained from the image of the junction region has the same reciprocal lattice peaks as do the FFTs obtained from the images of both backbone (upper-right inset) and branch (upper-left inset) regions, confirming the epitaxial branch-growth process.

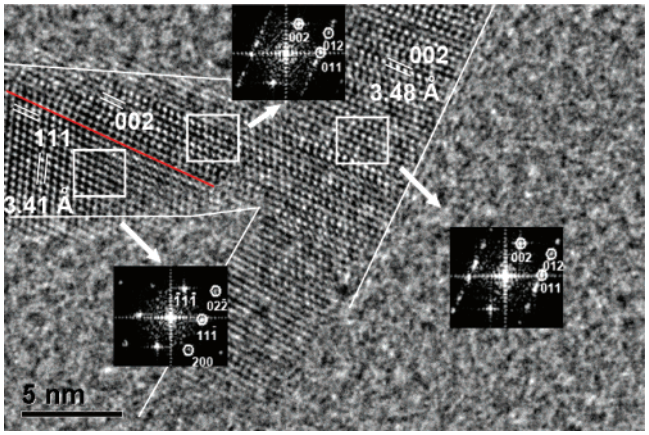

Figure 11. Representative HRTEM image of a single heterobranched CdSe−ZnSe NW with the CdSe backbone having a hexagonal crystal structure. The red line indicates the interface between the cubic and hexagonal crystal structures in the branch. The left, middle, and right insets show the 2D FFTs calculated from the corresponding images (indicated by squares) of the branch segment far from the junction, transitional branch segment, and backbone region, respectively. The [002] lattice−fringe spacing, 3.48 Å, measured from the backbone, agrees with that of CdSe, and the [111] lattice−fringe spacing, 3.41 Å, measured from the branch, is consistent with alloyed $Zn_{1-x}Cd_xSe$.

As noted above, another normally observed branching structure has a single branch exhibiting two different branching angles with respect to the backbone axis (see Figures 8a and 9a). HRTEM studies showed that this branching structure originated from the CdSe backbones possessing a hexagonal crystal structure. Figure 11 illustrates the HRTEM image of such a branching structure, as well as the corresponding FFTs obtained from the images of different regions. The indexed reciprocal lattices (Figure 11, right inset) confirmed that the backbone (∼6 nm in diameter) had a hexagonal crystal structure and the [002] direction was aligned with the backbone axis in the $[2\bar{1}0]$ zone axis. The FFT (Figure 11, middle inset) obtained from the image of the branch segment near the junction region demonstrated that this transitional segment also had a hexagonal

crystal structure with a growth axis along the $[0\bar{1}\bar{1}]$ lattice direction in the $[2\bar{1}0]$ zone axis, which was consistent with the epitaxial branch process. The angle between this transitional branch segment and the backbone axis determined from the reciprocal lattice peaks is 63.2°, consistent with the theoretical value 61.4° between $[0\bar{1}\bar{1}]$ and [002] directions in the $[2\bar{1}0]$ zone axis. The length of this transitional segment is ~15 nm. Interestingly, the remaining branch after the transitional segment had a cubic crystal structure, with the growth axis along the $[\bar{1}\bar{1}1]$ lattice direction in the [011] zone axis, as confirmed by the corresponding FFT (Figure 11, left inset). The angle between this cubic-structured branch and the hexagonal-structured backbone is 69.9°, determined from the reciprocal lattice peaks. This accounts for the above observed branching angle difference in the same branch with respect to the backbone axis. There is an interface (indicated by a red line in Figure 11) between two crystal phases in the branch. This interface is a junction between the (002) lattice plane from the hexagonal phase and the (111) lattice plane from the cubic phase, i.e., $(002)_{hexagonal}||(111)_{cubic}$. Note that the angle between the cubic-structured branch and the hexagonal-structured backbone is supposed to be 70.5° if there is a perfect epitaxial relationship at the interface of $(002)_{hexagonal}||(111)_{cubic}$ in the branch. Our experimentally measured angle, 69.9°, is consistent with the theoretical value, 70.5°, thus confirming a good epitaxial relationship of $(002)_{hexagonal}||(111)_{cubic}$ at the interface in the current case. This result is reasonable because the (111) facets of the cubic structure are atomically identical to the (002) facets of the hexagonal structure.[23] A cartoon depicting the orientation and growth directions of this heterobranched NW is provided in the Supporting Information (Figure S5).

We note that, in some cases, the measured angles between the cubic-structured branch and the hexagonal-structured backbone are several degrees away from 70.5°. An example of such a heterobranched NW is shown in Figure S6 (Supporting Information), in which the angle between the cubic-structured branch and the hexagonal-structured backbone is 63.7°, about 7° smaller than the predicted value of 70.5°. Presumably, this difference is due to the imperfect epitaxial relationship of $(002)_{hexagonal}||(111)_{cubic}$ at the interface in the branch, which might be caused by the slight twisting between two crystal structures and defect incorporation at the interface.

We surmised that, at an early stage, a ZnSe branch began to grow epitaxially from the CdSe backbone, with a considerable amount of Cd ions diffused into the branch region. Therefore, the early formed $Zn_{1-x}Cd_xSe$ branch segment would inherit the backbone's hexagonal crystal structure, leading to the transitional-section formation. With further branch lengthening and the gradual decrease in the amount of Cd ions diffused into the branch, the newly formed $Zn_{1-x}Cd_xSe$ branch segment would prefer to exhibit the cubic structure of ZnSe, resulting in the observed interface between the two crystal phases.

Finally, the optical properties of the CdSe−ZnSe heterobranched NWs were studied. Two evident excitonic features, arising from CdSe backbones (~650 nm) and ZnSe branches (~450 nm), respectively, were observed in the UV−visible absorption spectrum (Figure 12a) of the heterobranched NWs shown in Figure 8a. Both excitonic features were blue-shifted with respect to the corresponding bulk band gaps (~710 nm for CdSe and ~460 nm for ZnSe), due to quantum-confinement

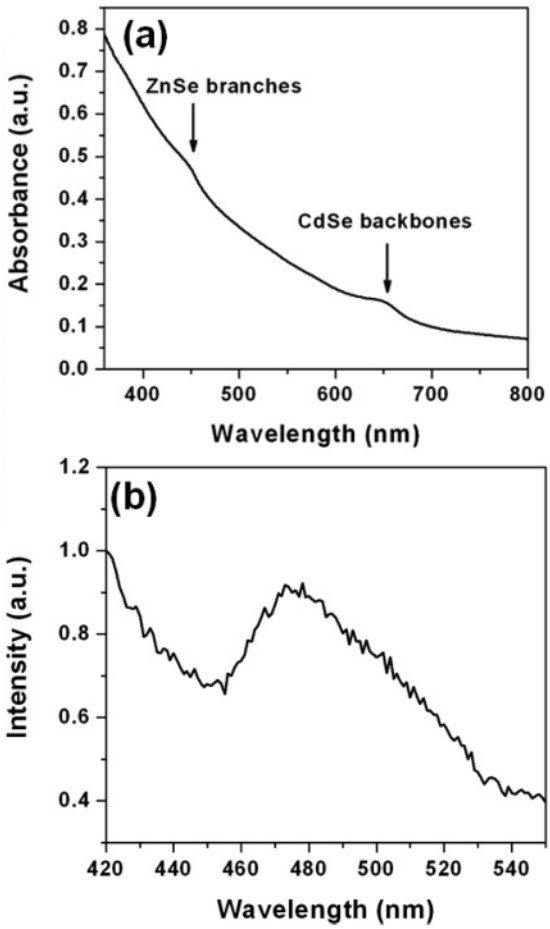

Figure 12. (a) UV−visible absorption spectrum of the heterobranched CdSe−ZnSe NWs shown in Figure 8a. The arrows indicate the first excitonic features arising from ZnSe branches and CdSe backbones, respectively. (b) PL emission spectrum of the same sample, showing the emission peak arising from the branches. The red shift of the emission peak relative to the bulk band gap of ZnSe was due to the alloyed $Zn_{1-x}Cd_xSe$ segment in the branch. The excitation wavelength was 340 nm.

effects. The PL spectrum (Figure 12b) of the same sample showed a weak and broad emission peak at ~480 nm, attributed to emission from branches. This emission peak was red-shifted compared to the bulk band gap of ZnSe (~460 nm), presumably due to the formation of alloyed $Zn_{1-x}Cd_xSe$ in the branch. We observed that the PL from the CdSe backbone NWs was quenched after PEI-coating, presumably by introduction of surface defects through the loss of TOPO, HDA, or TOP ligands. In a few cases, weak PL from the CdSe backbones was recovered in the CdSe−ZnSe heterobranched NWs, presumably by partial surface reconstruction in the presence of TOPO, HDA, and TOP ligands during branch growth. However, in most cases PL from the CdSe backbones was not observed in the heterobranched NWs. Future work is aimed to optimize reaction conditions to improve the PL intensities of these heterobranched NWs.

Conclusions

In this work, we have successfully synthesized colloidal homobranched ZnSe NWs and heterobranched CdSe−ZnSe NWs by applying a stepwise seeding strategy in the SLS growth process. An efficient approach involving PEI-coating and subsequent annealing has been developed to achieve a high-yield, firm attachment of secondary Bi seeds to the NW

backbones, which contributes to the high branching yield obtained in our experiments. The branching morphology, including the density, length, and diameter of branches, can be manipulated in a rational way by optimizing reaction conditions. Structural characterization by HRTEM and FFTs reveals that the single-crystalline ZnSe branches grow epitaxially from the backbone. Notably, two branching structures have been observed in the CdSe−ZnSe heterobranched NWs, due to the phase admixture existing in the CdSe NW backbones. Our approach should be successful for various semiconductor backbone NWs, provided that they are stable through the ligand-exchange reaction. Conceptually, the Bi-seed-deposition step and branch-growth process can be repeated one or more times to produce higher-order branched (hyperbranched) NWs. Such rationally designed NW assemblies are expected to open up many new opportunities for the fabrication of nanoscale electronic and photonic devices, due to their intrinsic complexity and dimensionality.

Acknowledgment. We thank Professor Richard Loomis for helpful discussions and the National Science Foundation (grant no. CHE-0518427) for support of this work. A.D. is grateful to the Washington University Graduate School of Arts & Sciences for a one-semester research fellowship.

Supporting Information Available: TEM and HRTEM images, branch-diameter distribution histogram, EDS spectra, and cartoon illustration. This material is available free of charge via the Internet at http://pubs.acs.org.

JA0737772